Plasmonics (2020) 15:2027–2032
https://doi.org/10.1007/s11468-020-01229-0

# Gold-Stabilized Gold–Silver Alloy Nanostructures as High-Performance SERS Substrate

Hang Li[1] · Hongmei Liu[1] · Youjian Qin[1] · Yunyun Mu[1] · Xiaohui Fang[1] · Tianrui Zhai[1] · Xinping Zhang[1]

Received: 14 May 2020 / Accepted: 29 June 2020 / Published online: 7 July 2020


## Abstract

Surface-enhanced Raman scattering (SERS) is a molecule-specific ultra-sensitive spectroscopic technique. With the development of portable Raman equipment, it has become possible to apply the SERS technique for rapid on-site detection. Therefore, the search for materials with excellent surface plasmon resonance (SPR) activity and high stability has become an important research focus in recent years. In this study, we successfully prepared plasmonic nanostructures with a large number of SERS "hotspots" using alloy nanoparticles (NPs) with tunable gold–silver mole ratios. These structures were composed of numerous narrow gapped gold–silver alloy NPs with diameters ranging from 10 to 100 nm. SERS property evaluation showed that the prepared alloy SERS substrates had good uniformity, and the performance of the substrates rapidly improved as the Ag content increased. Gold-stabilized Au–Ag alloy SERS substrates combine the high performance of the Ag SERS substrate and the excellent stability of Au. In addition, the wavelength of the SPR can be tuned by adjusting the mole ratio of Au and Ag to satisfy different excitation wavelengths. Thus, the Au–Ag alloy SERS substrates we prepared show good comprehensive performance. The lowest concentration of rhodamine 6G that can be homogeneously detected by the prepared $Au_1Ag_8$ alloy substrate is $5 \times 10^{-12}$ M, and the enhancement factor is $5.1 \times 10^8$. Finite-difference time-domain (FDTD) theoretical calculations further confirmed our experimental results and theoretically demonstrated the unique properties of the Au–Ag alloy SERS substrates.

**Keywords** Surface-enhanced Raman scattering (SERS), · Surface plasmon resonance (SPR), · Au–Ag alloy · Finite-difference time-domain (FDTD)

## Introduction

Surface-enhanced Raman scattering (SERS) spectroscopy is an ultra-fast, non-destructive analysis technique based on the fingerprint vibration information of the molecule to be analyzed. Its detection limit is in the order of single molecule [1–4]; therefore, it has become an important inspection method in fields such as guaranteeing food safety [5], preventing drug abuse [6, 7], preserving the environment [8, 9], and fighting terrorism [10]. With the rapid development of portable Raman spectrometers, it has been possible for SERS to be applied for rapid on-site detections [11]. Therefore, searching for high-performance and low-cost SERS active materials or structures has become an important research subject. Multicomponent nanostructures have recently attracted attention as they provide novel functions not available in single-component materials or structures [12–15]. For example, Y. H. Liu et al. demonstrated a Ag–Ti alloy substrate in which 2% Ti could be sacrificed against oxidation and corrosion, protecting Ag in harsh environments and ensuring the long-term stability of the SERS substrate [12]. T. C. Gong et al. reported a hybrid substrate of octahedral Au nanocrystal–filled Ag nanohole arrays for SERS applications. This hybrid structure showed higher SERS sensitivity than either of the single structures owing to the plasmonic coupling effect generated by the hybrid structure [13]. K. G. Li et al. fabricated porous Au–Ag hybrid nanoparticle arrays. These structures exhibited a long shelf-life in an ambient environment and showed better SERS activities than simple Ag structures owing to the large number of "hotspots" and the hybrid

**Electronic supplementary material** The online version of this article (https://doi.org/10.1007/s11468-020-01229-0) contains supplementary material, which is available to authorized users.

✉ Hongmei Liu
hmliu@bjut.edu.cn

✉ Xinping Zhang
zhangxinping@bjut.edu.cn

[1] Institute of Information Photonics Technology, School of Physics and Optoelectronics, Faculty of Science, Beijing University of Technology, Beijing 100124, People's Republic of China

nanostructure [14]. Multicomponent nanostructures exhibit better SERS activity than any of the single components; however, their preparation is generally complicated and costly, which significantly limits their practical applications.

In 2014 we proposed a facile route for the assembly of gold nanoparticles (NPs) into SERS substrates [16]. The substrates show high uniformity, and the relative standard deviation of the SERS signal intensity on the substrate is less than 5.4%, and the global enhancement factor is $1 \times 10^7$. This preparation method can be used to prepare SERS substrates with large areas at low cost, and the preparation process is easy to control. However, since the preparation of solution dispersible alloy nanoparticles was not mature at that time, the assembly of Au–Ag alloy SERS substrates was challenging. In our recent work, we improved the Brust method and successfully fabricated Au–Ag alloy NPs, which showed good dispersion in organic solvents. By using a solution processing method, Au–Ag alloy SERS substrates with different Au and Ag mole ratios could be synthesized. By evaluating the SERS sensitivity, we found that the alloy SERS substrates showed good performance and stability. The lowest detection concentration with high uniformity was $5 \times 10^{-12}$ M for $Ag_8Au_1$ samples. Compared with the pure Ag SERS substrates, the substrates of the alloy can be stored for a long period. The unannealed sample can be stored for a long time without being oxidized owing to the protection of the 1-hexanethiol monolayer that bonds to the surface of the metallic NPs.

## Preparation of SERS Substrates with Different Gold–Silver Ratios

Brust and co-workers have been developing a method for the efficient synthesis of alkyl thiol-stabilized gold nanoparticles since 1994 [17]. However, it is not possible to synthesize Au–Ag alloy NPs in large quantities using this method because the AgX (X = $Br^+$ or $Cl^-$) precipitate forms when $AgNO_3$ reactant is mixed with tetra-n-octylammonium bromide (TOAB) and hydrogen chloroaurate ($HAuCl_4$), making it difficult to achieve a homogeneous reaction. Through our research we found that if a certain amount of alkyl-thiol compound is added in advance, the formation of AgX precipitate in the solution can be prevented. Based on this finding, we modified the Brust method and successfully synthesized Au–Ag alloy NPs in large quantities.

Tetraoctylammonium bromide (1.50 g, 2.75 mmol) and 1-hexanethiol (0.36 g, 3.04 mmol) were dissolved in 80 mL of toluene, then $AgNO_3$ (0.066 g, 0.39 mmol) in 2 mL of water was added to the mixture. When the light-yellow precipitate had completely transferred into the organic phase, $HAuCl_4 \cdot 4H_2O$ (0.32 g, 0.78 mmol) in 1 mL of water was added. Finally, 20 mL of freshly prepared aqueous sodium borohydride (0.28 g, 7.4 mmol) solution was rapidly injected into the flask, and the solution quickly became purple. The aqueous phase was removed after 4 h of reaction. The remaining organic solvent was removed using a rotary vacuum evaporator. The black solid product was washed four times with methanol using centrifugal methods and dried under vacuum. Finally, the black powder with a Au-to-Ag mole ratio of 2:1 was obtained. By changing the mole ratio of silver nitrate and gold chloride, nanoparticles with different Au and Ag mole ratios could be obtained. By dissolving 40 mg of alloy nanoparticles in 0.5 mL of chloroform, a colloidal solution of 80 mg/mL was prepared. The colloidal solution was then spin-coated onto a silicon wafer at 2000 rpm and annealed in a muffle furnace at 200 °C for 20 min to remove the 1-hexanethiol ligands and obtain clean Au–Ag alloy nanostructures.

## Morphology of SERS Substrates with Different Gold-Silver Ratios

The surface morphology of the metallic nanostructures was characterized using a Hitachi S-4800 scanning electron microscope (SEM). Figure 1a–d shows typical SEM images of SERS substrates assembled from metallic alloy NPs with different Au–Ag compositions and reveals large-scale assemblies of closely packed NPs. The corresponding high-resolution SEM images of these assemblies are shown as insets. We found that the alloy nanoparticles on the substrates vary in size, with diameters in the range 10–100 nm, and there are numerous narrow nanogaps between the particles. Comparing samples with different composition, we found that the diameter of the nanoparticles on the substrate increased gradually with increasing Ag content. For example, the diameter of the $Au_1Ag_2$ alloy nanoparticles was between 10 and 50 nm, while the diameter of the $Au_1Ag_8$ alloy nanoparticles was in the range 40–100 nm. This is because silver has a lower melting point than gold, and the increased proportion of silver reduced the melting point of the alloy NPs, so they fused into larger particles after annealing.

In the SERS phenomenon, intense electromagnetic fields occur in gaps narrower than 10 nm between adjacent metallic NPs, which are called “hotspots” [18]. Reliable fabrication of homogeneous and high density “hotspots” at low cost remains a challenge. We found that the nanogaps between the NPs in the structures we prepared were so small that SEM was unable to clearly distinguish them (Fig. 1a–d), indicating that there were many enhancement “hotspots” buried in these structures.

## Properties of SERS Substrates with Different Gold-Silver Ratios

### SERS Performance of the Substrates with Different Gold–Silver Ratios

To evaluate the SERS properties of the plasmonic structures, Raman experiments were conducted using rhodamine 6G

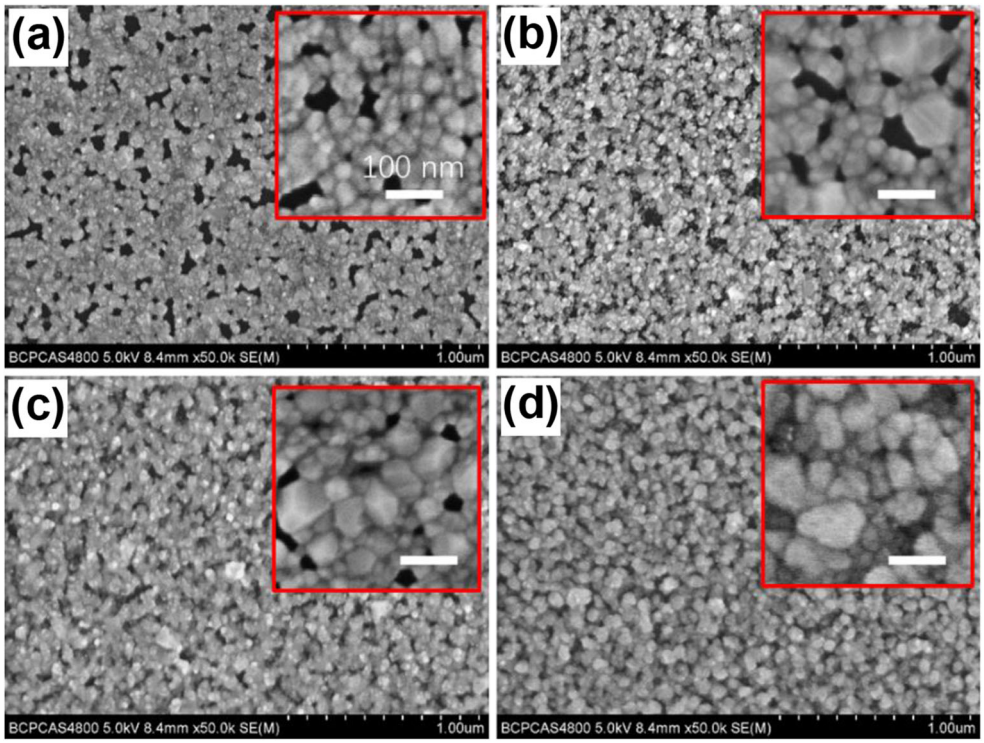


**Fig. 1** Morphology of plasmonic nanostructures composed of different gold and silver mole ratios: **a** $Au_1Ag_1$, **b** $Au_1Ag_2$, **c** $Au_1Ag_4$, and **d** $Au_1Ag_8$

(R6G) as the probe molecule because of its well-established vibrational features. In order to make sure all of the substrates exhibited distinguishable SERS signals under the same test conditions, we used a solution of $1 \times 10^{-6}$ M. First, we drop cast 20 μL of the solutions on the prepared 0.25 $cm^2$ SERS substrates, and then characterized them using a WITec Alpha300A confocal Raman spectrometer equipped with 532 nm and 633 nm excitation laser sources. A × 50 objective (numerical aperture NA ¼ 0.8) was used for the measurements, and the light spot at the focus was approximately 811 nm in diameter for the 532 nm laser and 965 nm for the 633 nm laser. A 0.5-mW laser power was used to continuously scan 50 × 50 points with a step of 1 μm on an area of 50 × 50 $\mu m^2$, the integration time of each point was 0.5 s, and the "mapping" data were used to show the fluctuation of the SERS signal at each point. The average of the 2500 scan spectra was used as the final measurement result. The SERS spectra from the substrates with different Au-to-Ag mole ratios are longitudinally distributed in Fig. 2. When the 532-nm laser was used for excitation, significant increases in the intensity of the spectra were observed when the proportion of Ag was increased, and the greatest intensity was observed for the pure Ag substrate. However, when the SERS substrates were excited with a 633-nm laser, the SERS signal did not increase with increasing Ag content, but instead decreased slightly (Fig. S1). We attribute this to the 633-nm incident light not matching the SPR wavelength of the Au–Ag alloy NPs. The 532-nm light matches well because when the Ag content increases, the SPR wavelength of the Au–Ag alloy NPs blue shifts. To confirm our speculation, we measured the extinction spectra of SERS substrates with different compositions, as shown in Fig. S2. A fairly broad extinction spectrum was observed for all the samples owing to the small gaps between the adjacent NPs leading to strong plasmonic coupling. Even so, the blue shift trend of the extinction spectra could still be observed in Fig. S2.

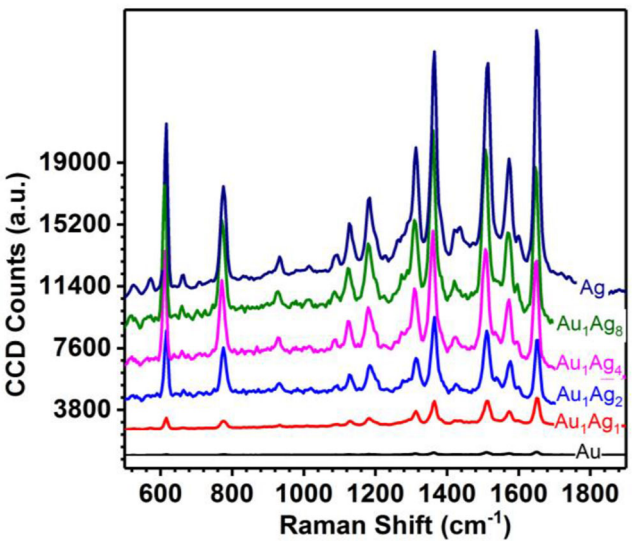


**Fig. 2** Longitudinally distributed SERS spectra of plasmonic alloy nanostructures with different Au–Ag mole ratios. The probe molecule was R6G, the concentration was $1 \times 10^{-6}$ M, and the excitation light source was a 532-nm laser

## Stability of the Gold–Silver Alloy Substrates

An ideal substrate must be stable for long periods of time; therefore, the stability of the Au–Ag alloy SERS substrates is an important issue that needs to be evaluated. We investigated the stability of the alloy substrates by comparing the properties of freshly prepared SERS substrates with those of substrates stored in air for several weeks. Figure 3 shows the SERS performance variation of Au, $Au_1Ag_8$, and Ag substrates with time. Figure 3a shows that the gold substrate had a very stable SERS performance. Its SERS spectrum did not decrease in intensity with increasing storage time, but gradually increased, accompanied by the gradual increase of the fluorescence of R6G. We estimate that the fluorescence enhancement was due to the adsorption of air molecules on the surface of the Au NPs, which weakened the fluorescence quenching of R6G by metal. However, after only 1 week, the SERS signal intensity of the Ag and $Au_1Ag_8$ substrates decreased to nearly a quarter of that of the freshly prepared samples. This is because the oxidation of Ag changes the chemical composition of the surface of the Ag and alloy nanoparticles, thereby reducing the surface enhancement properties of the substrate. As the oxide layer thickened, the intensity of the SERS spectrum of the Ag substrate rapidly decreased, and the SERS signal became very weak after 4 weeks. Encouragingly, the intensity of the SERS spectrum of the alloy substrate stabilized after 2 weeks and no longer decreased, which is attributed to the stabilizing effect of Au preventing further oxidation of the substrates. By comparing Fig. 3a–c, we found that the $Au_1Ag_8$ alloy SERS substrates had both better stability than Ag substrates and better SERS performance than Au substrates. Thus, the performance of the optimized alloy substrate combined the advantages of the Au and Ag SERS substrates and exhibited the best properties. Further experiments showed that the unannealed samples could be stored for a much longer time without being oxidized than annealed samples owing to the antioxidant effect of the 1-hexanethiol ligands on the surface of the NPs. Therefore, doping gold into silver to form alloy SERS substrates and annealing when required for use are effective methods for improving the stability of this kind of SERS substrate.

## Homogeneity of the Alloy SERS Substrates

Uniformity is another significant concern for SERS substrates. To characterize the homogeneity of SERS enhancement on the substrates, the main vibrations of R6G were measured using the "mapping" mode. Up to 6400 spectra were collected in the image shown in Fig. 4a, which is based on the intensity distribution of the Raman peak at 1364 $cm^{-1}$ over an area of $50 \times 50$ $\mu m^2$. We found that the bright and dark spots were homogeneously distributed on the image. The average SERS spectrum over the entire mapping area was calculated and is shown as a black line in Fig. 4b. We found that the C–C–C ring in-plane bending of R6G at 613 $cm^{-1}$, the out-of-plane bending at 769 $cm^{-1}$, and the ring breathing (RB), such as aromatic C–C stretching at 1183, 1312, 1364, 1512, and 1648 $cm^{-1}$, and $\nu$(C–H) at 1127 $cm^{-1}$ were enhanced at all test points, indicating excellent SERS activity on the substrate. The maximum and minimum SERS intensity signals were also picked from the 6400 spectra and are shown as blue and red lines in Fig. 4b, respectively. We found that there were no points for which no signal was detected over the entire measurement area, which further illustrates the high uniformity of the SERS substrate. Fluctuations in signal amplitude are mainly due to the uneven spread of R6G molecules on the surface of the substrates as a result of drop casting. The global enhancement factor (EF) was calculated according to the method reported in reference [19], and the average EF was $1.1 \times 10^5$ at 1364 $cm^{-1}$. The lowest concentration of R6G solution that our Raman spectrometer can uniformly detect is $5 \times 10^{-12}$ M for the $Au_1Ag_8$ alloy SERS substrates, and the spectra are shown in Fig. 4c. These spectra show that the RB vibration mode of R6G was significantly enhanced, and the ring bending modes were just detectable. For the maximum, minimum, and average intensity SERS spectra, there was no significant fluctuation at low concentrations, indicating that the R6G molecules were uniformly distributed at low detection concentration. The global enhancement factor was calculated to be $5.1 \times 10^8$ for 1650 $cm^{-1}$ peaks.

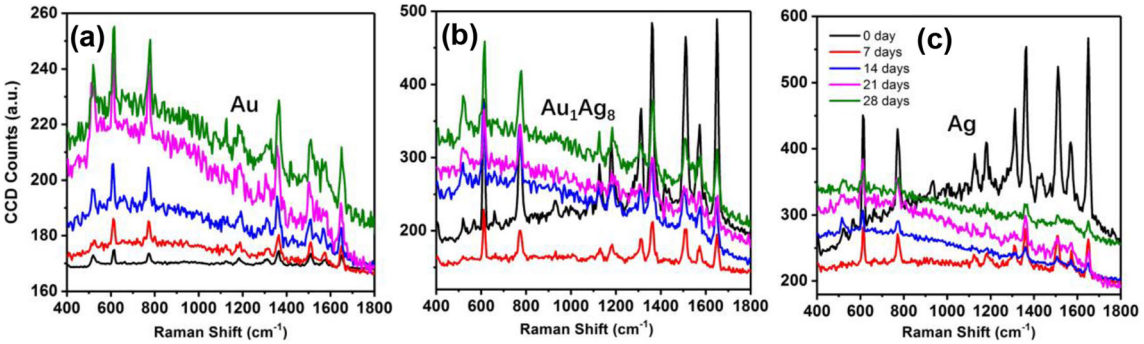


**Fig. 3** SERS spectra of R6G loaded **a** Au and **b** $Au_1Ag_8$ and **c** Ag SERS substrates. The substrates were stored in air for 0–4 weeks

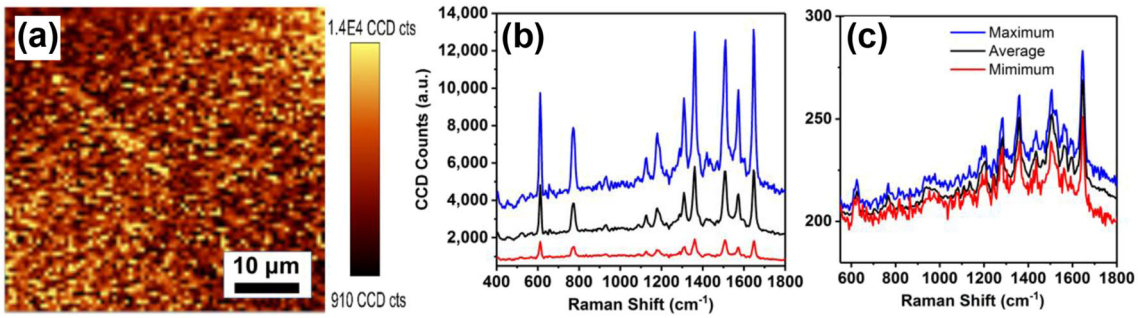


**Fig. 4** **a** The "mapping" image of a 50- × 50-μm$^2$ area for the Raman vibration at 1364 cm$^{-1}$ of $1 \times 10^{-6}$ M R6G obtained from an $Au_1Ag_8$ alloy SERS substrate. **b** The maximum (blue), average (black), and minimum (red) SERS spectra over the entire mapping area in (**a**). **c** SERS spectra of $5 \times 10^{-12}$ M R6G obtained from the $Au_1Ag_8$ alloy SERS substrate

## Theoretical Calculation of the Near-Field Electric Field Intensity

Finite-difference time-domain (FDTD) is an efficient technique that can calculate the electromagnetic fields within a compact spatial region and can also obtain the scattered and/or radiated far fields via near-to-far-field transformation [20, 21]. Here this method was used to simulate the intensity of the localized electromagnetic fields between the metallic NPs. The following equation was then used to calculate the local enhancement factor ($EF_{loc}$) [18]:

$$EF_{loc} = |E_{loc}(\omega_i)|^4 / |E_0(\omega_i)|^4$$

We found that the $EF_{loc}$ is proportional to the fourth power of local electric fields ($E_{loc}$) at the incident frequency ($\omega_i$). The simulations were carried out for NPs with different Au–Ag mole ratios. The geometry of the Au–Ag metal nanostructures we calculated is shown in the inset of Fig. 5. The nanoparticles are both 80 nm in diameter, and the distance between them is 4 nm. We first calculated the $E_{loc}$ between the particles at excitation wavelengths of 532 and 633 nm, and then the local electromagnetic enhancement factor and described them in Fig. 5. We found that the enhancement factor strongly depended on the composition of the NPs for the given geometry with incident irradiation of 532 nm. The EFs increased rapidly with increasing silver content. When the silver mole fraction was over 60%, the $EF_{loc}$ increased exponentially with the increase of silver content. However, under 633 nm irradiation the local EFs of the same geometry decreased gradually with increasing silver mole fraction. When the silver mole ratio was over 50%, the EFs were almost unchanged. The significant difference between the different excitation wavelengths theoretically demonstrates that the SPR wavelengths of Au–Ag alloy NPs match the 532-nm irradiation well. Therefore, in the silver-dominated plasmonic structures, the SPR can be effectively excited by 532 nm rather than 633-nm laser. When effective excitation occurs, the incident and scattered Raman photons are both strongly enhanced. The maximum of the local enhancement factor is $1 \times 10^8$ for 532 nm irradiation in the silver-dominated structure, which is 2 orders of magnitude higher than that of 633 nm. To further confirm the effect of the composition of metal NPs on the SPR wavelength, we theoretically calculated the extinction spectra of the NPs with different Ag mole compositions, as shown in Fig. S3. It can be seen that the extinction peaks were significantly blue-shifted as the proportion of silver increased. This means that by changing the composition of the Au–Ag alloy, the SERS substrates were able to meet the needs of different excitation wavelengths in practice.

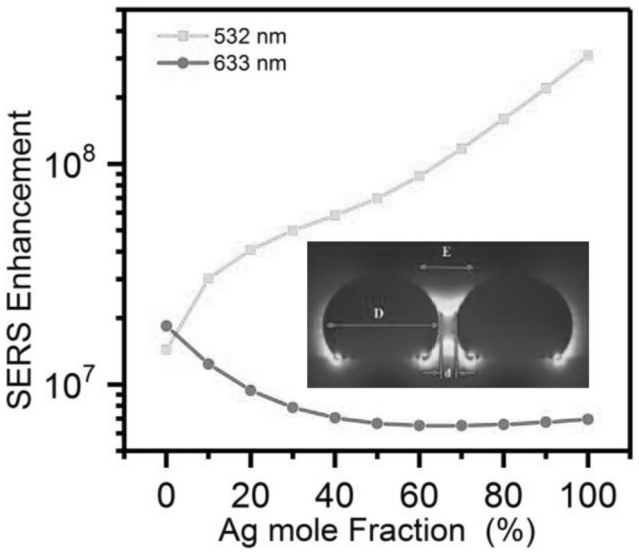


**Fig. 5** FDTD simulations of the Ag mole fraction–dependentlocal enhancement factor of the Au–Ag alloy nanospheres, with incident wavelengths of $\lambda = 532$ nm and 633 nm. Inset shows the calculated geometry of the nanospheres: the diameter of the NPs is $D = 80$ nm, and the gap between them is d = 4 nm

## Conclusions

In conclusion, we successfully assembled Au–Ag alloy SERS substrates with uniform "hotspot" distribution using a solution processing method. The SERS performance of the alloy

substrates increased significantly with the increase of the silver content. The lowest R6G concentration that the $Au_1Ag_8$ substrate could homogeneously detect was $5 \times 10^{-12}$ M, and the corresponding global enhancement factor was $5.1 \times 10^8$. Increasing the doping ratio of silver causes the SPR wavelength of the alloy NPs to blue shift; therefore, the 532-nm excitation light became the optimal excitation wavelength. The pure Ag SERS substrate exhibited unexpectedly high SERS performance, while the pure Au SERS substrate exhibited excellent stability. The alloy SERS substrates exhibited the advantages of both Ag and Au, showing good stability and excellent performance. It is also thought to be possible to tune the SPR wavelength of the alloy SERS substrates by adjusting the ratio of Au and Ag to adapt them to different excitation wavelengths. The FDTD theoretical calculation results were consistent with our experimental results, which further confirm the unique properties of the Au–Ag alloy SERS substrate.

**Funding Information** The authors received financial support from the National Natural Science Foundation of China (61735002, 61575007 and 11304005) and the Beijing Educational Commission (KZ202010005002 and KM201510005030).

## References

1. Nie SM, Emory SR (1997) Probing single molecules and single nanoparticles by surface-enhanced Raman scattering. Science 275:1102–1106
2. Kneipp K, Wang Y, Kneipp H, Perelman LT, Itzkan I, Dasar RR et al (1997) Single molecule detection using surface-enhanced Raman scattering (SERS). Phys Rev Lett 78:1667–1670
3. Yang SK, Dai XM, Stogin BB, Wong TS (2016) Ultrasensitive surface-enhanced Raman scattering detection in common fluids. Proc Natl Acad Sci U S A 113:268–273
4. Cui L, Zhang YJ, Huang WE, Zhang BF, Martin FL, Li JY, Zhang KS, Zhu YG (2016) Surface-enhanced Raman spectroscopy for identification of heavy metal arsenic(V)-mediated enhancing effect on antibiotic resistance. Anal Chem 88:3164–3170
5. Lee SY, Ganbold EO, Choo J, Joo SW (2010) Detection of melamine in powdered milk using surface-enhanced Raman scattering with no pretreatment. Anal Lett 43:2135–2141
6. Burr DS, Fatigante WL, Lartey JA, Jang W, Stelmack AR, McClurg NW et al (2020) Integrating SERS and PSI-MS with dual purpose plasmonic paper substrates for on-site illicit drug confirmation. Anal Chem 92:6676–6683
7. Fernandes de Oliveira Penido CA, Tavares Pacheco MT, Lednev IK, Silveira L (2016) Raman spectroscopy in forensic analysis: identification of cocaine and other illegal drugs of abuse. J Raman Spectrosc 47:28–38
8. López-Tocón I, Otero JC, Arenas JF, Garcia-Ramos JV, Sanchez-Cortes S (2011) Multicomponent direct detection of polycyclic aromatic hydrocarbons by surface-enhanced Raman spectroscopy using silver nanoparticles functionalized with the viologen host lucigenin. Anal Chem 83:2518–2525
9. Koh CS, Lee HK, HanX SHY, Ling XY (2018) Plasmonic nose: integrating the MOF-enabled molecular preconcentration effect with a plasmonic array for recognition of molecular-level volatile organic compounds. Chem Commun 54:2546–2549
10. Chou A, Jaatinen E, Buividas R, Seniutinas G, Juodkazis S, Izakea EL et al (2012) SERS substrate for detection of explosives. Nanoscale 4:7419–7424
11. Lin S, Hasi W, Lin X, Han S, Xiang T, Liang S, Wang L (2020) Lab-on-capillary platform for on-site quantitative SERS analysis of surface contaminants based on Au@4-MBA@Ag core−shell nanorods. ACS Sens 5:1465–1473
12. Liu YH, Wu H, Ma LW, Zou SM, Ling YH, Zhang ZJ (2018) Highly stable and active SERS substrates with alloy nanorods. Nanoscale 10:19863–19870
13. Gong TC, Luo YF, Zhang HB, Zhao CW, Yue WS, Pu MB, Kong WJ, Wang C, Luo X (2020) Hybrid octahedral Au nanocrystals and Ag nanohole arrays as substrates for highly sensitive and reproducible surface-enhanced Raman scattering. J Mater Chem C 8:1135–1142
14. Li KG, Liu GJ, Zhang S, Dai YQ, Ghafoor S, Huang WX, Zu ZW et al (2019) A porous Au–Ag hybrid nanoparticle array with broadband absorption and high-density hotspots for stable SERS analysis. Nanoscale 11:9587–9592
15. Yang H, Li BQ, Jiang XB, Shao JY (2019) Hybrid nanostructure of $SiO_2$@Si with Au-nanoparticles for surface enhanced Raman spectroscopy. Nanoscale 11:13484–13493
16. Liu HM, Zhang XP, Zhai TR, Sander T, Chen LM, Klar PJ (2014) Centimeter-scale-homogeneous SERS substrates with seven-order global enhancement through thermally controlled plasmonic nanostructures. Nanoscale 6:5099–5105
17. Brust M, Walker M, Bethell D, Schiffrin DJ, Whyman R (1994) Synthesis of thiol-derivatized gold nanoparticles in a two-phase liquid-liquid system. J Chem Soc Chem Commun 1994:801–802
18. Ding SY, You EM, Tian ZQ, Moskovits M (2017) Electromagnetic theories of surface-enhanced Raman spectroscopy. Chem Soc Rev 46:4042–4076
19. Le Ru EC, Blackie E, Meyer M (2007) Surface enhanced Raman scattering enhancement factors a comprehensive study. Phys Chem C 111:13794–13803
20. Chen Y, Wang J, Xu T, Liu M, Liu J, Huang H, Ouyang F (2020) FDTD simulation of the optical properties for a gold nanoparticle-over-nanosheet hybrid structure. Curr Appl Phys 20:391–399
21. Qin F, Chen X, Yi Z, Yao W, Yang H, Tang Y, Yi Y, Li H, Yi Y (2020) Ultra-broadband and wide-angle perfect solar absorber based on TiN nanodisk and Ti thin film structure. Sol Energy Mater Sol Cells 211:110535